LEAD ARTICLE

Acta Cryst. (1995). A**51**, 237–252

X-ray Microscopy

BY D. SAYRE AND H. N. CHAPMAN

Department of Physics, State University of New York, Stony Brook, NY 11794, *USA*

(*Received* 19 *May* 1994; *accepted* 17 *October* 1994)

Abstract

The subject of X-ray microscopy (high-resolution X-ray imaging of general nonperiodic structures), an area in which much progress has been made in recent years, is reviewed. The main techniques are briefly described. Achievable performance levels, which for many years were highly speculative, can now be understood with fair accuracy in terms of basic X-ray and specimen properties, and techniques have progressed to the point where actual results are nearing those levels. In terms of specimen size and imaging resolution, X-ray microscopies lie between electron and light microscopy, and are thus suited to imaging extremely large and complex structures; in addition, they demand little or no specimen preparation, and can be used to observe local composition and chemical state as well as structure. Thus X-rays, which have played the leading role in imaging crystallizable materials, may also prove to be highly valuable in the imaging of very large non-crystalline structures. Throughout the treatment, attention is paid to the relationships connecting the subject with X-ray crystallography.

Introduction

The question considered in this paper is: in the absence of specimen periodicity, what level of high-resolution X-ray imaging of the internal structure of matter is possible, and by what methods? To anticipate the answer, Fig. 1 briefly shows the position of X-ray microscopy, as it has emerged in recent years, in relation to the established imaging methods.

With regard to the techniques by which the imaging is accomplished, it will be noted that X-ray crystallography uses diffraction analysis as its central imaging methodology, while electron and light microscopies use focusing optics as their principal technique. There is thus a tendency to progress from diffraction to focusing technology as one moves upward and to the right in Fig. 1. This tendency is partially but not completely maintained in X-ray microscopy, where both techniques are

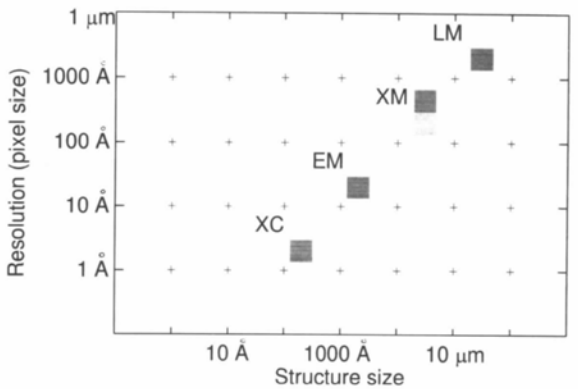

Fig. 1. 'Zoom' in imaging. The current imaging methods for internal structure (XC = X-ray crystallography, EM = electron microscopy, LM = light microscopy) give reasonable coverage through most of the range from atomic resolution up, except in the gap falling somewhat above 1 μm structure size. It is here that the X-ray microscopies (= XM) fall. The diagram is intended to reflect the properties of the methods when imaging large biological structures. As to why the methods have the resolutions they do: EM uses energetic particles and its resolution is mainly limited by the radiation damage that they produce; LM uses low-energy particles and is diffraction limited; XC uses high-energy particles but is able to operate at or near the diffraction limit of X-rays because of the assistance relative to damage provided by the specimen periodicity (see §III). Finally, XM uses more highly energy depositing particles than EM; its estimated approximate damage-limited position is shown by the lightly shaded square in the figure. At present (darker square), it is still slightly in its historical position of being instrumentation limited in its resolution but needs only moderate further improvement to reach the damage-limited condition, after which techniques to combat specimen damage will be a primary factor in any further improvement in resolution. For the horizontal position occupied by XM, see Fig. 5.

David Sayre received his doctorate in 1951 *from Oxford University, where he studied with Professor Dorothy Hodgkin. He has contributed to direct-method phasing techniques in crystallography, to compiler and virtual-computer techniques in computation, and in later years to X-ray microscopy.*

Henry Chapman received his PhD at The University of Melbourne, Australia, in 1992. *His thesis on X-ray optics using capillary arrays won him the Australian Institute of Physics Bragg Gold Medal for the best thesis written in* 1992/93. *Since then he has been a postdoctoral associate at SUNY Stony Brook, developing imaging techniques in X-ray microscopy.*

David and Henry have been working together on soft X-ray diffraction from nonperiodic structures [*see Section* II.4(*a*) *of the article*].

used. At the present time, the two techniques, diffractive and focusing, turn out not to differ greatly in terms of resolution in X-ray microscopy, and do not need to be distinguished in Fig. 1.

This paper consists of a main text, which might be read alone on a first reading, plus more detailed *Notes* which are found at the end of the paper. See, for example, *Note* 1.

Finally, a word about the approach taken in this paper. A major goal of the paper is not only to describe (briefly) X-ray microscopy but also, insofar as is possible, to derive the subject from basic physical considerations, with the aim of providing it with as reliable a foundation as possible. The reader will find these aspects of the paper mainly in §I (including Fig. 5 and *Notes* 2 and 3) and §III; it is primarily in these sections that the position of XM in the imaging series is derived. A second goal is to provide a parallel view of X-ray crystallography, with the aim of showing how, from a common starting point, the two widely different places of XC and XM in the imaging series develop out of the presence and absence of specimen periodicity. This aspect is summarized in *Note* 9.

I. Preliminaries: imaging, reactions of X-ray photons

1. *Imaging*

The basic view taken in this paper is that imaging is the determination of the locations of reactions occurring in a specimen. A map of the locations then gives – on the principle that the specimen matter is where the reactions are – an image of the specimen. High-resolution imaging means high-accuracy localization of the reactions; this accuracy in turn may be limited by fundamental constraints on localizability, such as the Heisenberg positional uncertainty (which yields the familiar half-wavelength resolution limit in crystallography and the diffraction limit in microscopy), or it may be limited by shortcomings of the instrumentation or by structural damage in the specimen caused by the imaging reactions. One may if desired then divide high-resolution imaging into imaging of periodic or near-periodic specimens (crystallography) and imaging of specimens that are not periodic or near-periodic (microscopy). Finally, X-ray microscopy and crystallography image *via* reactions produced in the specimen by incident X-rays.

When several types of reaction occur in a specimen, more than one image can be formed, increasing the information obtainable about the specimen. As will be seen, with X-rays in the energy range of principal interest in the present subject (wavelength roughly 10–50Å), the atoms of the specimen are the principal reaction sites. They act in this capacity in not one but several major ways: as X-ray photon removal sites, and as particle emission sites emitting several classes of photons and electrons. In addition, each atomic species (carbon, nitrogen *etc.*) has its own individual cross sections for the removal and for the several emission behaviors, and these atomic cross sections are further individualized by the way in which they vary with the energy of the photons present and with the chemical state of the atom. Thus, it is clear that if it were possible to carry around, within the interior of the specimen, an ultra-small particle-detection laboratory while at the same time controlling the X-ray environment of the specimen, it would be possible to extract a great wealth of information concerning the structure, composition and chemistry of the specimen.

In reality, of course, the ultra-small laboratory does not exist and the problem faced in imaging technologies is that of finding ways of working from outside the specimen to obtain an approximation of the potentialities just sketched. Fortunately, methods have developed over the years for doing this in a number of ways. These include: (1) determining the spatial distribution of particles exiting the specimen using a high spatial resolution detector placed close to the specimen (microradiography or contact microscopy); (2) as above, but generally more accurately, devising a focusing system to direct exiting particles to different points on a detector according to their points of origin in the specimen (transmission microscopy, also referred to as conventional or imaging microscopy); (3) use of a focusing system to deliver the incident particles to the specimen as a well localized reaction-producing probe (scanning microscopy); and (4) analysis of the interference patterns formed by exiting coherently scattered particles, permitting accurate location of the coherent scattering sites without a corresponding requirement for high-accuracy detectors or optics (diffractive methods). §II will discuss today's X-ray versions of these four basic types in more detail. In addition, the possible variations in illumination, reaction type, detection and analysis are such that there are potential new methodologies to be considered as well. §II thus also includes (5) a sampling of some additional techniques of possible future importance. Finally, §IV will present some of the current work in X-ray microscopy in adding compositional and chemical information to the structural information obtained about specimens.

2. *Reactions of X-ray photons*

The discussion of imaging just given makes clear the need to know the reactions that X-ray photons can induce in microscopy specimens. In the range of photon wavelengths that are of principal interest here, the most frequent reaction is photoabsorption, in which a photon is captured by an atom, the state of the atom is disturbed, and the atom responds by emitting a lower-energy electron plus secondary electrons and/or photons. Energy is absorbed by the structure and there is possible breakage of chemical bonds. Also present is Rayleigh (or elastic) photon scattering, in which the atom, instead

of emitting an electron, is able to rid itself of the energy of the captured photon by emitting a photon of the same energy as that of the captured photon. Here there is minimal disturbance of the electronic structure of the atom and energy is not absorbed. The overall result, taking the two reactions together, is that the major reaction locations are at the atoms of the specimen and that at these locations there is (*a*) removal of incident photons, (*b*) emission of electrons and photons of lower energy than the incident photons, and (*c*) coherent scattering of the incident photons. As will be seen, all three of these effects can be used for reaction location and hence for imaging.

As can be seen, effect (*a*) arises from both photoabsorption and Rayleigh scattering and effect (*b*) from photoabsorption. Less obviously, (*c*) also arises from both reactions, in part through the direct contribution of coherent photons by Rayleigh scattering but also through the scattering produced by the photoabsorbing atom acting as a diffracting obstacle for photons. Thus, it is customary to define for (*c*) an atomic complex coherent scattering factor f embracing both contributions and having the non-dissipative (Rayleigh) component as its real part f_1, and the dissipative (photoabsorption) component as its imaginary part f_2. [See Henke, Gullikson & Davis (1993) for a tabulation of f_1 and f_2 for all atoms and for photon energies from 50 to 30 000 eV or wavelengths 250 to 0.4 Å.] In extended bodies, the complex scattering factor gives rise to a complex index of refraction, with f_1 and f_2 contributing, respectively, phase shift and attenuation of the transmitted X-rays. As will be seen in the next section, both phase-shift-based and attenuation-based X-ray microscopies have been developed.

A third reaction, Compton (or inelastic) scattering, becomes important at wavelengths below about 10 Å. Here, a photon is captured by an electron, a photon of lower energy is emitted and energy is absorbed by the specimen. Compton scattering thus contributes a further effect of type (*b*). Some work has been done on Compton-based imaging (Harding, Strecker & Tischler, 1983/84), but development of the technique is hampered by the higher energy of the photons involved, for which high-resolution focusing systems are not currently available.

Further information on the photon reactions is given in *Notes* 2 and 3. Finally, before turning to the techniques of X-ray imaging in more detail, it will be helpful to have in mind the connections between the several basic methodologies [(1)–(5) earlier] and the detectable reaction effects (*a*)–(*c*). Thus, method (4) (diffractive methods) clearly links to effect (*c*). Almost as clearly, method (1) (microradiography) links to effect (*a*); a moment's thought reveals that a reasonable way to detect photon removal is with an on-axis photon detector and that method (1) effectively uses a spatial array of such detectors to map the photon removals in the specimen. Method (3) (scanning) can be seen to have full flexibility, linking to (*a*) with the use of an on-axis photon detector, or to (*b*) or (*c*) with the use of off-axis detectors for the particular particles being monitored. Method (2) (focusing of exiting particles) can also link with (*a*), (*b*) and (*c*), although not always as easily as method (3), since (2) requires the focusing as well as the detection to be matched to the particles being detected. Lastly, the several methods of type (5) that are discussed in this paper link mainly with effect (*c*).

II. X-ray microscopy techniques

This section briefly describes the main techniques of X-ray microscopy as they have developed to date and indicates their resolution limitations other than radiation damage to the specimen. The methods are treated in the same order (1)–(5) in which they were outlined in §I. The question of radiation damage as a limiting factor on resolution is treated in §III.

1. *Microradiography (contact microscopy)*

The discovery of X-ray radiography in 1896 showed that a position-sensitive detector could detect the locations of photon removal occurring in an object with which it was in close contact. Following this, radiographs of small objects were produced and examined under the light microscope to obtain a useful early form of X-ray microscopy. The resolution of the technique, however, remained limited to that of the light microscope until the work of Ladd, Hess & Ladd (1956), who examined very high resolution radiographs recorded as relief images on ammonium dichromate or polyvinyl chloride under the electron microscope. The usual technique today employs poly(methyl methacrylate) (PMMA) as the high-resolution recording medium for the radiograph (Spiller & Feder, 1977). In addition, atomic force microscopy rather than electron microscopy is beginning to be employed for more quantitative read-out of the PMMA (Tomie *et al.*, 1991; Cotton, Dooley, Fletcher, Stead & Ford, 1992).

Surface roughness of the PMMA imposes a limit of about 100 Å on the current resolution of the method (Shinozaki, Cheng & Lin, 1992). For most specimens, however, a larger loss of resolution arises from the fact that not all parts of a specimen of finite thickness can be in close contact with the detector, leading to blurring of the radiograph by diffraction. The resolution for imaging a layer of the specimen at a distance h from the recording medium is approximately $(h\lambda)^{1/2}$, where λ is the wavelength of the X-rays used. For a 3 μm thick specimen, with $\lambda = 30$ Å, the resolution with which the topmost layer is imaged is approximately 1000 Å. Thus, although for thin specimens microradiography can be one of the higher-resolution X-ray microscopy methods, it is not generally a high-resolution XM method.

The technique has a higher importance than might be inferred from its resolution alone, however. This arises from its ease of set-up and considerable versatility. Of particular interest is the convenience with which it can be used with flash X-ray sources for stop-motion imaging and as a means of fast image capture before the onset of radiation damage (Skinner *et al.*, 1990; Fletcher, Cotton & Webb, 1992).

In the thin-specimen case, the details of the shadow cast in the very near field by a photon-removing atom have been calculated by Sayre (1988).

2. *Focusing of exiting particles*: *transmission (or conventional or imaging) microscopies*

Despite the traditional view that X-rays cannot be focused, the topic of focusing systems for X-rays has today become an extensive subject (Michette 1986). The principal techniques employ diffraction from microstructures that have been especially designed and fabricated to have diffraction functions appropriate to the directing of photons in the desired manner. Historically, it was necessary to wait for high-precision microfabrication techniques before these devices could be produced, explaining the long delay in their availability for microscopy. The most frequently used systems to date are very small versions of the Fresnel zone plate or related structures; these are lenslike transmission devices having *f*/numbers which in a few cases today reach values of about *f*/10 for 25 Å X-rays, giving imaging resolutions of about 250 Å (David *et al.*, 1992; David, Fay, Medenwaldt & Thieme, 1994; Attwood, 1994). Most modern zone plates are phase zone plates (Kirz, 1974) to increase efficiency. Some use has also been made of reflective devices, both grazing and normal incidence.

It appears likely that the resolution obtainable with basically two-dimensional focusing elements, such as zone plates, may by now have nearly reached its limit. For this reason, attention is now being directed to several types of three-dimensional focusing structures (Ray, 1954; Aristov, 1994; Maser & Schmahl, 1992; Shealy, Wang, Jiang, Jin & Hoover, 1992), which may in time be developable to resolutions of 100 Å or better. At such resolutions, these structures could bring about the estimated damage-limited resolution situation pictured in Fig. 1. Further improvement in resolution, at least for biological specimens, would then depend upon finding ways to reduce radiation damage to the specimen.

Despite the success of diffractive structures in focusing, it should be noted that present devices pose two somewhat troublesome problems in the context of microscopy. Photon losses are typically high (currently 90% or more), in the case of transmission microscopy (but not scanning microscopy) causing unnecessary radiation dosage to the specimen. However, it has been shown by Maser (1994) that it should be possible to fabricate zone plates with efficiency approaching 50% and so reduce the dose to the specimen. In addition, most of the devices are chromatic (*i.e.* require refocusing on change of wavelength). Since wavelength change is a powerful way of gaining additional information in X-ray microscopy (see §IV), it would be more convenient if the devices were achromatic.

A number of transmission X-ray microscopes (TXMs) have been built (see *e.g.* Schmahl *et al.*, 1993; papers in Erko & Aristov 1994); microscopes of this type are likely, just as in electron and light microscopy, to be very durable and successful types in X-ray microscopy. As noted near the end of §I, transmission microscopes have considerable versatility in the reaction effects that they can image from, though on the whole somewhat less than do the scanning microscopes. The principal versions to date image on the basis of photon removal or as phase-contrast microscopes [see item 5(*b*) later in this section]. As noted above, because of losses in the currently available focusing devices for X-rays, these tend to expose the specimen to extra radiation dosage. Their resource in combating this is that, being parallel devices, they have, like microradiography, a high rate of image capture and are thus compatible with flash X-ray sources. A table-top flash X-ray transmission microscope is in commercial development (Schmahl *et al.*, 1992).

3. *Focusing of incident particles*: *scanning microscopies*

Just as in other types of microscopy, the existence of focusing devices also allows the construction of scanning X-ray microscopes (Jacobsen *et al.*, 1994). Scanning microscopes are more complex than transmission microscopes owing to their requirement for a precision scanning stage with accompanying computer control. Images, however, are precise and digital and can be based, through appropriate choice of detector, on almost any product or effect of the reactions being produced in the specimen; for these reasons, scanning microscopes have to date been principally responsible for the advanced techniques discussed in §IV. Two main types of scanning microscopes exist today: STXMs (scanning transmission X-ray microscopes primarily equipped with photon detectors); and SPEMs (scanning photoemission microscopes primarily equipped with electron detectors). An advantage of scanning, already noted, is that inefficiencies of the focusing system are not translated into increased radiation dosages on the specimen. However, any noise from the source or scanner will cause pixel-to-pixel variations that will require increased dose. Image acquisition, being serial, cannot be extremely high speed. Current imaging times for the Brookhaven STXM and SPEM (from a fraction of a minute to several minutes) are not inconvenient for ordinary purposes, but cannot approach the nanosecond-scale times – important for image capture prior to radiation damage – that can be done with contact or imaging microscopy. Nevertheless, at the level of the pixel, the dwell time can be as brief

as a few milliseconds, which is often fast enough that damage does not affect the image.

4. *Diffractive methods*

The preceding methods are based primarily on observing the loss of photons from the incident photon stream or on the observation of lower-energy emission particles. The present section takes up two methods that, like X-ray crystallography, image on the basis of the addition rule for coherent scattering (*Note* 3).

(*a*) *The analog of X-ray crystallography for nonperiodic structures.* As is well known, given a single finite structure and a crystal composed of repeated occurrences of the structure, the diffraction pattern Ω_c of the crystal will consist of a greatly amplified Bragg sampling of the pattern Ω_s of the original nonperiodic structure; in view of the sampling, Ω_s (although more difficult to measure because of its lower amplification) actually contains information not present in Ω_c. Hence, in cases where a crystal is not available but the single finite structure is, it is plausible that its pattern Ω_s may make a very suitable substitute for Ω_c as a basis for imaging the structure. Because of its faintness, Ω_s does not extend to as high a resolution as the crystal pattern. Even so, the possibility exists of a highly important extension of X-ray crystallography, although at reduced resolution. The extension can be thought of as the X-ray crystallography of 'crystals' consisting of a single asymmetric unit or 'single-copy' or 'single-a.s.u.' X-ray crystallography.

Based on these thoughts, an early form of which was expressed by Sayre (1980), gradual progress has been made in developing the technique for observing diffraction patterns from single instances of micrometer-size specimens. Work has concentrated on using single biological cells as the diffracting objects. The first patterns of this type were obtained from single small diatoms (Yun, Kirz & Sayre, 1987) and some years later, with an improved apparatus, from single ordinary small cells (Sayre, 1991). Current work is being done with single sperm and muscle cells (Chapman *et al.*, 1993).

Basically, the technique requires an intense source of illumination plus design precautions to ensure that (*a*) the photons incident on the specimen are narrowly confined in energy and direction, and (*b*) no particles other than photons diffracted by the specimen reach (or are recorded by) the detector. The former condition (Sayre, Yun & Kirz, 1988) is to produce a single well defined sphere of reflection and the latter is to allow the faint diffraction pattern to be seen above noise; together these are to prevent the continuous nature and the faintness of the diffraction pattern from interfering with observation of the pattern. Fig. 2 shows in schematic form the approach currently in use in this work.

To complete the overview of the method, it is necessary to consider the phasing of the diffraction pattern to allow computation of the image. The following approach has not yet been tried but it is hoped to begin a trial soon.*

It has been known for the last decade that a combination of oversampling in Fourier space and a reasonably good envelope in direct space makes a powerful phasing situation. In two or higher dimensions, sampling the diffraction intensity at twice the Bragg frequency of any lattice on which the structure can be repeated without overlap suffices in principle to determine the phasing (Hayes, 1982; Bates, 1982). (Here, twice the Bragg frequency means 4× oversampling in 2D, 8× in 3D *etc.*) An extensive literature on computer phasing algorithms based on this result now exists (see *e.g.* Idell, 1994).

A moment's thought will show that diffraction with non-crystallograpic specimens is very well suited to this phasing situation. Oversampling is available through the continuity of the diffraction pattern, and because of the nonperiodicity the specimen possesses an envelope that can be observed directly in a light, X-ray or electron microscope. Should the method prove successful, non-

* *Note added in proof*: Early tests of the approach carried out with simulated 2D data sets have now given encouraging results.

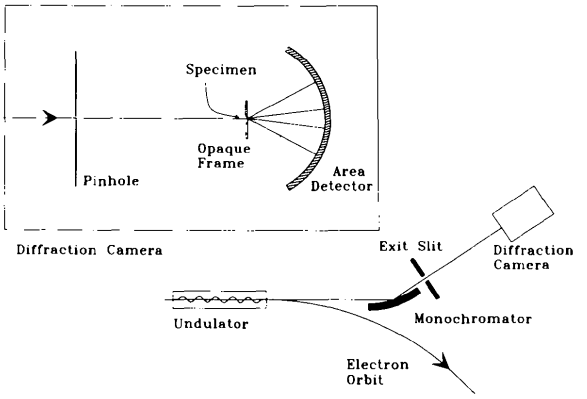

Fig. 2. Experimental set-up for observing the diffraction pattern Ω_s of a non-crystallographic specimen. The intense, sharply forward-pointing, undulator radiation plus the monochromator provide a stream of photons in a narrow range of energy and direction; the opaque frame of the specimen-bearing window (the window opening may typically be 0.25 × 0.25 mm) protects most of the detector from photons other than those diffracted by the specimen. In addition, in the usual case where there are multiple specimens on the specimen window, a small (15 μm) pinhole is placed upstream of the window to allow a single specimen to be illuminated, and an x–y positioner for the window is provided to allow placing of the desired specimen in the beam. To date, angular positioners for the specimen, to allow full 3D collection of Ω_s, have not been provided; for a stationary specimen (collecting on a single reflecting sphere), typical exposure times are 10 min. The apparatus is evacuated to allow soft X-rays (typically to date 18–25 Å wavelength) to be used, and specimens have been air-dried. There is no obstacle, however, to maintaining specimens in the future in a wet or frozen state by adding proper environmental chambers and/or cooling systems. The detector used to date has been special soft-X-ray-sensitive silver halide film (Kodak XUV T-100). In the next design, this will be replaced by a back-illuminated CCD detector to allow lower detector noise and faster data acquisition.

crystallographic structure analysis could be a quite rapid technique of imaging, with diffraction data being passed to a computer on an almost real-time basis for application of the phasing algorithm and image presentation. It may be noted, finally, that the images will in general be complex valued (thus adding to the information content), corresponding to the fact that the coherent scattering factor in the soft-X-ray region has generally a significant imaginary part f_2 as well as a real part f_1 (see §I.2).

On the resolution issues, in a damage-free world the technique would have no essential resolution limitation short of the diffraction limit. If that situation existed, resolutions as high as 10 Å, using 20 Å wavelength X-rays, could be envisaged; *i.e.* this technique would not be limited by shortcomings in X-ray technology. In the real situation, however, damage does exist and dominates the resolution situation; this is seen in the fact that the largest resolution to date to which diffraction has been observed for a single biological cell is of the order of 140 Å (70 Å in the case of a single diatom), but not 10 Å. See §III for further discussion.

It should be noted that the measurement of an accurate oversampled data set does not come free of charge; increased counts are needed, implying a need for increased exposure and an attendant increase in damage to the specimen. The actual quality of the phasing that will be obtainable with the oversampling method is also uncertain at the present time, especially if less than full 3D data are available.

(*b*) *X-ray holography.* The second diffractive technique available to X-ray microscopy is X-ray holography, which differs from the preceding in using a different approach to phasing. In holography, reference photons are allowed to travel along additional coherency-preserving photon paths from source to detector. With appropriate choice of the additional paths, the phasing of Ω_s can be found from the modified interference pattern that results.

In the case of crystallographic structures, holographic ideas have faced a chronic difficulty: the process of examining any appreciable amount of the diffraction pattern normally requires a mechanical motion (crystal rotation), which destroys the necessary precision of the spatial relationship between the diffracted and reference photon paths. It has therefore been necessary for crystallographers to devise special forms of holography based on reference paths that move with the crystal, as in paths involving heavy atoms or anomalous scatterers within the crystal, or multiple (n-beam) diffraction. If the structure is non-crystalline, however, the continuity of the diffraction pattern allows appreciable amounts of the pattern to be examined without motion and the problem disappears. The ability to see between the Bragg spots thus simplifies the phase problem, whether by oversampling or by holography.

With the disappearance of the motion problem, the more usual ways of adding paths in holography can be used. In particular, X-ray holographic imaging has been successfully carried out by both Gabor and Fourier holography. In the former (see *e.g.* Jacobsen, Howells, Kirz & Rothman, 1990), the added photons have been photons in the same central beamline maximum as that which illuminates the specimen and, in the latter (McNulty *et al.*, 1992), they have been photons emerging from the focus of a zone plate placed in that maximum. A recent brief summary of the subject has been given by McNulty (1994).

Although holography adds still further phasing assistance in carrying out diffractive imaging, it should be noted that it reintroduces technology as a resolution-limiting factor. (In Gabor holography, resolution is limited by the spatial resolution of the detector observing the hologram and in Fourier holography by the sharpness of the focus of the zone plate that supplies the reference photons.) In addition, the reference photons are a source of added noise in the recording of the diffraction signal. For these reasons, it is not yet certain how the two approaches (holography and the nonperiodic form of crystallography) will ultimately work out in comparison with one another.

5. *Other methods*

Although the above are the major techniques of X-ray microscopy at present, there are several other methods that present interesting possibilities.

(*a*) *Microradiography at several distances.* The problem of diffraction blurring that occurs with thicker specimens in contact microradiography can in principle be overcome by modifying the experimental set-up to measure the field intensity with high spatial resolution detectors at several distances from the specimen. The method really constitutes another example of phasing by intensity oversampling and was proposed by Sayre (1986), who devised a phasing algorithm based on propagator theory (Goodman, 1968) and used it successfully in tests employing simulated field intensity data. The theory has subsequently been greatly expanded by Nugent (1992). The problem in applying the technique is the very high spatial precision and registration required in the detector data. It is possible that the use of atomic force microscopy as the method of detector read-out may allow some progress to be made on this problem.

(*b*) *Phase-contrast microscopy.* X-ray phase-contrast imaging (imaging a specimen *via* its properties as a phase-modifying object) was proposed by Schmahl & Rudolph (1987) (see also Rudolph, Schmahl & Niemann, 1990). These methods can either produce images of a specimen for which the contrast is a linear combination of the real and imaginary parts of the complex transmittance of the specimen, as in Zernike phase contrast, or images for which the contrast is given by the phase gradient, as in differential phase contrast. Zernike phase contrast is most easily implemented in a transmission

microscope by advancing the phase of the unscattered light by 90° before interfering, at the image plane, with the light scattered by the object. Differential phase contrast is ideal for a scanning microscope using a split detector as an optical lever to measure refractive-index gradients as well as photoabsorption.

The technique was first implemented, using a Zernike phase-contrast technique with a transmission X-ray microscope, by Schmahl, Rudolph & Guttmann (1988). See also Schmahl *et al.* (1994) for a more recent implementation. Differential phase contrast has been demonstrated in a scanning microscope by Palmer & Morrison (1992), and Chapman (1995) has discussed implementations of phase-contrast methods on a scanning microscope. An advantage of phase contrast is that the contrast may be much higher than in photoabsorption maps, and hence the required dose may be less by a factor of six (Schmahl *et al.*, 1994) depending on the wavelength and specimen geometry. Also, this mode can be carried out at shorter X-ray wavelengths (above authors and Jacobsen, 1992), allowing thicker specimens to be imaged.

(*c*) *Dark-field imaging, combination of scanning and diffraction.* X-ray dark-field imaging (use of Rayleigh-scattered photons in a scanning or transmission microscope) is an additional imaging technique with the advantage of low-background counting compared with imaging with transmitted photons. The technique can be implemented with off-axis illumination in a transmission microscope or off-axis detection in a scanning microscope. In the scanning configuration, a large number of dark-field images can be obtained in one scan by using a multiplicity of off-axis detectors such as a CCD array. Since the scattered photons are predominantly coherently scattered photons, the successive CCD patterns are a set of scanned microdiffraction patterns. Recently, it has been shown in the EM literature that, given such a set of patterns, maps equivalent to those of the more usual diffraction methods can be obtained through Wigner-distribution deconvolution methods (Rodenburg & Bates, 1992). Although the equivalences present here are intriguing, it is not yet clear whether this newer route to such maps will have advantages over the §II.4 methods. One of us (HC) has recently begun experimenting with such methods using the Brookhaven scanning microscope.

(*d*) *Coded-aperture imaging.* In coded-aperture imaging (CAI), a specimen is incoherently illuminated, a patterned mask is placed between the specimen and a downstream two-dimensional detector and the radiation exiting from the specimen throws a complex patterned shadow on the detector; the specimen image is decoded from the recorded shadow by optical or numerical techniques (Skinner, 1988). Generally, the resolution of the image is set by the smallest feature size of the mask. The theory has lately been generalized by Nugent, Chapman & Kato (1991) to allow wavelengths of radiation that are comparable to the mask feature size, and for which diffraction of the radiation by the mask must be taken into account. In this form, the theory can cover the possible use of CAI in X-ray microscopy and finds that for both coherently scattered and transmitted photons the processing performed by CAI is equivalent to that of a transmission X-ray microscope; in fact a transmission XM can be considered as CAI with a special (zone plate) type of mask. Certain differences exist, however: accurate placement of source, object, and optics is not in general required in CAI, and 'focusing' can be done in the reconstruction step (a possible advantage in flash imaging). Likewise, effective numerical apertures may be larger in CAI, permitting better coding of three-dimensional information concerning the specimen; and through use of a uniformly redundant array (Fenimore & Cannon, 1978) as the mask, object information can be more efficiently coded than with a zone plate, allowing a smaller detector array to be used.

III. Radiation dosage in imaging; specimen damage as a limitation on resolution

§II described X-ray microscopies as they might exist in a world that is free of radiation damage and showed that the major techniques (with the exception of the non-periodic analog of X-ray crystallography) are currently limited to about the 300 Å resolution level by X-ray optical technology, but also appear to be capable of reaching perhaps the 100 Å level in the next few years. In the present section, the influence of radiation damage on resolution is taken up, and rough estimates are produced of achievable resolution in the presence of damage. In addition, with the arrival of better X-ray microscopes, useful experimental data on the subject of damage have begun to be available. The basic result of this section is that, at resolutions not very much higher than those available today, damage considerations will become the major limiting factor in X-ray microscopy.

First, estimates are derived of the radiation dosages delivered to specimens in the course of imaging by different methods and at different resolutions. Estimates are then given of the dosages at which damage becomes perceptible in specimens of different types under different circumstances. These two considerations, when taken together, lead to estimates of maximum resolution under a variety of imaging methods, specimen types and imaging circumstances. The estimates, although approximate, agree quite well with experimental evidence where that evidence is available. The section concludes with a few remarks on methods for increasing specimen tolerance of dosage.

The estimates of imaging dosage as a function of imaging method and resolution are obtained as follows. Four quantities are considered: V = volume of resolution element, R = number of reactions required to be located per resolution element for sufficiently low noise imaging, E = energy deposition in the specimen per located

reaction, C = coherency gain, which may exceed unity in imaging based on coherent scattering (see *Note* 3). Thus, assuming that specimens have unit density,

$$\text{Dosage} = D = RE/VC.$$

If the transverse imaging resolution is d, then for all single-orientation imaging methods the volume of the basic resolution element is approximately $V = d^4/\lambda$ (see *Note* 6).

As a first example, consider the two-dimensional imaging based on locating the photoabsorption reaction, using 30 Å wavelength X-rays. R may be taken to be 10^4 to keep noise at the 1% level (see *Note* 4). From Fig. 7 (*Note* 5), E is approximately $10^{2.6}$ eV. With $C = 1$, the result is, for a resolution of d Å

$$D = 10^{8.1}/d^4 \text{ eV Å}^{-3} = 10^{18.4}/d^4 \text{ rad}$$

(1 rad = 0.01 Gy). If, however, the imaging is performed *via* Zernike phase contrast, Schmahl *et al.* (1994) have shown that the dose may be reduced by a factor of six, so that

$$D = 10^{17.6}/d^4 \text{ rad}.$$

As another example, consider stationary-specimen imaging of a nonperiodic specimen *via* coherent scattering, using 23 Å X-rays. Again, $R = 10^4$, $V = d^4/\lambda$ and, from Fig. 7, $E = 10^{6.7}$ eV. Finally, C, the coherency gain, is the number of atoms in the resolution element (the atoms in the resolution element scatter approximately in phase to scattering angles corresponding to resolution d); allowing a volume of 20 Å^3 per atom, $C = [10^{-1.3}\text{ Å}^{-3}]d^4/\lambda$. The result is

$$D = 10^{14.7}/d^8 \text{ eV Å}^{-3} = 10^{25}/d^8 \text{ rad}.$$

If one wishes to consider full three-dimensional imaging in this case, one may add a further factor M, referring to the necessity of carrying out a number of stationary-specimen diffraction experiments to fill in the full three-dimensional pattern. With the estimation $M = 10^2$ [which may be an overestimate given a theorem of dose fractionation by Hegerl & Hoppe (1976)], the result is $D = 10^{27}/d^8$ rad.

As a final example, one may take the three-dimensional imaging of a macromolecular crystal by X-ray crystallography, using 0.5 Å X-rays and assuming 10^{12} unit cells in the crystal. Here, $R = 10^4$, $E = 10^{4.8}$ eV, V and M are as above and C is as above but with an additional amplification factor of 10^{12}, independent of resolution d, owing to the periodicity (see *Note* 7). The result is

$$D = 10^{-0.5}/d^8 \text{ eV Å}^{-3} = 10^{9.8}/d^8 \text{ rad}.$$

These results are plotted in Fig. 3.

Turning now to the relation between dosage inflicted and damage done, recent work by Bennett, Forster, Buckley & Burge (1993), Williams *et al.* (1993), Schneider (1994) and Jacobsen (private communication) has begun to reveal a situation roughly as follows. At approximately 10^6 rad, loss of cell function develops slowly (over minutes or hours following the exposure) in living biological cells; this can include ultimate death of the cell. At approximately 10^7 and $10^{7.5}$ rad, slow XM-observable structural changes (*i.e.* changes visible in subsequent images of the cell) start to occur in living cells and in wet lightly fixed (0.1% glutaraldehyde) cells, respectively. At 10^8 and $10^{8.5}$ rad, structural changes which are fast enough to affect the appearance of first XM images occur in wet 0.1% and 1% glutaraldehyde-fixed cells, respectively. (The 10^8 rad level is that highlighted in Fig. 3 and used for the estimate of damage-limited resolution in Fig. 1.) At exposures as

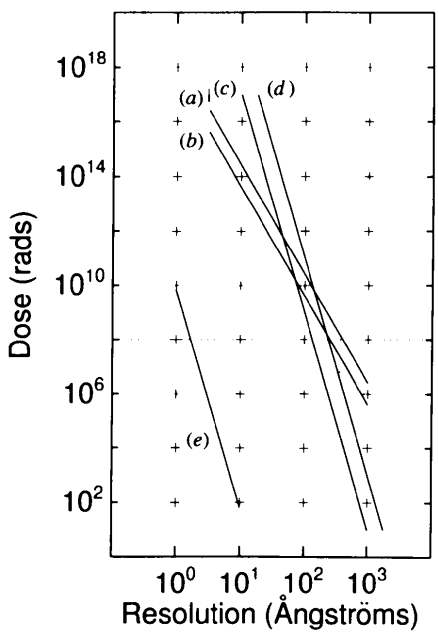

Fig. 3. Estimated imaging dose as a function of desired resolution for several X-ray imaging methods: (*a*) 2D photoabsorption-based microscopy; (*b*) 2D phase-contrast-based microscopy; (*c*) 2D imaging of a non-crystallographic specimen by diffraction or holography; (*d*) same for 3D; (*e*) 3D large-molecule crystallography. The curves suggest that, at the 100 Mrad level, X-ray microscopy methods (*a*)–(*d*) will show resolutions in the 100–400 Å range and that macromolecular crystallography (*e*) will show resolutions in the 2 Å range. (The method gives similarly reasonable estimates for electron microscopy.) Where these indications have been testable to date, *i.e.* (*a*), (*b*), (*c*) and (*e*), they are in reasonable agreement with experiment. The slopes of the curves suggest that, on damage-limited grounds, (*c*), (*d*) may ultimately be best suited to low-dosage medium-resolution imaging and (*a*), (*b*) to higher-resolution imaging. The fact that a simple theory without free parameters gives indications that come out well for both crystallography and microscopy suggests that the techniques are not as different as their positions in the imaging series may suggest and that they can be regarded as two aspects of a single subject. (For further comments, see *Note* 8.)

high as $10^{9.4}$ rad, damage has not been XM-observed in dried chromosomes. Note, however, that the dosages referring to XM-observable structural change are likely to decrease as X-ray microscopy resolution increases.

The above data refer to imaging under ordinary circumstances. By changing the circumstances, however, possibilities exist for lowering the damaging effect of dosage. These have not yet been adequately tested in terms of X-ray microscopy, but nevertheless deserve mention. Thus, Bennett, Forster, Buckley & Burge (1993) and Williams *et al.* (1993) have considered the use of chemical cell protectants and have shown small beneficial effects from the use of free-radical scavengers in wet chromosome and myofibril specimens. A second possibility is very high speed imaging. Here, Solem & Baldwin (1982), using inertial confinement theory, concluded that biological material, if imaged with an X-ray flash of the order of 10^{-12} s duration, will remain positionally unchanged to an accuracy of 100 Å for the duration of the exposure, and will remain unchanged to higher accuracy if the flash is shorter. Experimentation to date has been limited (see references in §II.1) but leaves intact the possibility that much of the damage-limited resolution problem in XM may be relieved through this technique, although at the high cost of obtaining only one image per specimen, since the specimen does not survive after the exposure. Finally, a third possibility is imaging at low temperatures. This has not as yet been tested in XM, but experience in X-ray crystallography and electron microscopy suggests (Hope, 1990; Echlin, 1992) that, by working at liquid-nitrogen temperatures, dosages corresponding to given damage levels may be increased by two to three orders of magnitude over the room-temperature dosages given above for wet biological materials, and by roughly a factor of five for dry materials. This also agrees with results of a model of specimen damage in X-ray microscopy by Schneider (1994). From these considerations, it appears that techniques for imaging at higher dosages, and hence at higher resolutions, may have a significant future role to play in XM.

IV. More advanced imaging. X-ray microspectroscopy and compositional and chemical information from X-ray microscopy

Thus far in this paper, photon reactions have been located and images formed but the images have not been studied as a function of the incident photon energy. The present section briefly considers this important merging of microscopic and spectroscopic ideas, in which the X-ray photon, acting as it does as a sensitive probe of the atomic state, can be used to gather quantitative information on the composition and chemistry of a specimen on a very small spatial scale. The treatment is brief, since the subject is still relatively new, real progress having begun primarily with the arrival of the X-ray scanning microscope, an instrument that is particularly suited to this work, since images are acquired in digital form, whereupon quantitative analysis of the specimen properties can be made pixel by pixel. The subject appears to be sufficiently important even today, however, that the future may see a large part of X-ray microscopy actually carried out as microspectroscopy.

Most of the work to date has centered on the spectroscopy of the photoabsorption reaction, although both coherent and Compton scattering will probably be fertile fields in the future as well. Elemental sensitivity is achieved by utilizing the large variation in the photoabsorption cross section of an element near the absorption edge. Given two images of the same field, one below and one above the absorption edge, the difference will show the spatial distribution of that element. This method has been used successfully to image calcium in human bone and cartilage; see *e.g.* Buckley *et al.* (1992).

Near an absorption edge, resonances occur in the photon/atom interactions as the photon energy is brought to match the energies of quantized electronic states in the specimen [Fig. 4(*c*) (iii)]. The spectral variation of the absorption cross section that results is known as near-edge X-ray absorption fine structure (NEXAFS) or X-ray absorption near-edge structure (XANES). This spectral structure is quite specific to the chemical environment of an element; that is, the molecular or covalent bonds that are present and the orientation of those bonds relative to the polarization of the incident X-rays. Thus, Ade *et al.* (1992) obtained images of polymer blends and biological materials at X-ray wavelengths corresponding to various resonances near the carbon *K* edge; different phases of the blends could be identified and phase compositions determined. Contrast between protein and DNA was seen and images obtained showing localization of DNA in metaphase chromosomes. More recent work of this type on protein/DNA has been done by Zhang *et al.* (1994) and on cartilage by Buckley, Bellamy, Khaleque, Downes & Zhang (1994). Ade & Hsiao (1993) have also exploited the dependence of the NEXAFS on geometrical orientation of the specimen relative to the electric field vector of the incident polarized X-rays to perform X-ray linear dichroism scanning microscopy. The intensity of a resonant transition is a maximum when the electric field is parallel to the direction of the bonds and varies as the cosine squared of the angle between them. By collecting on-resonance images of the transmission of a specimen at various azimuthal angles, information can be found on the degree of alignment and average orientation of bonds. This was done for thin sections of Kevlar fibers, which showed radially distributed aromatic groups of the polymer fibers.

Other effects of photoabsorption on which compositional and chemical-state analysis can be based are emission of lower-energy X-ray photons (X-ray fluorescence) or lower-energy electrons. Compositional information can be found from the spectrum of emitted

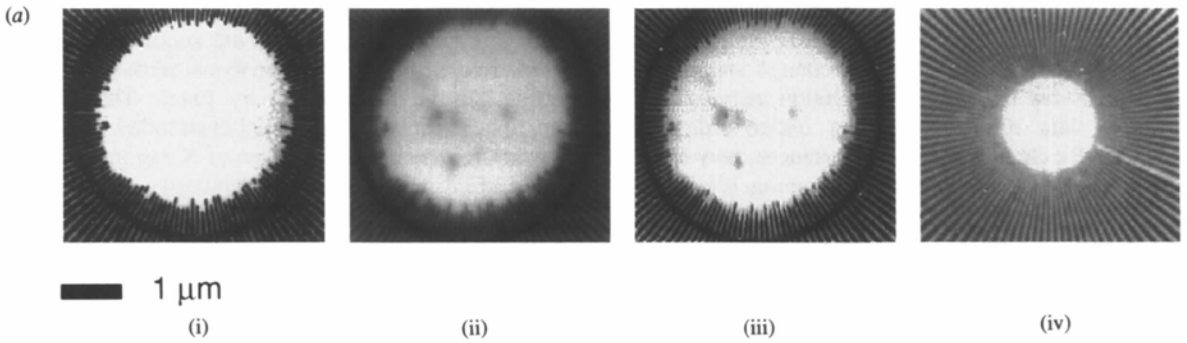
(a)
1 μm
(i)
(ii)
(iii)
(iv)

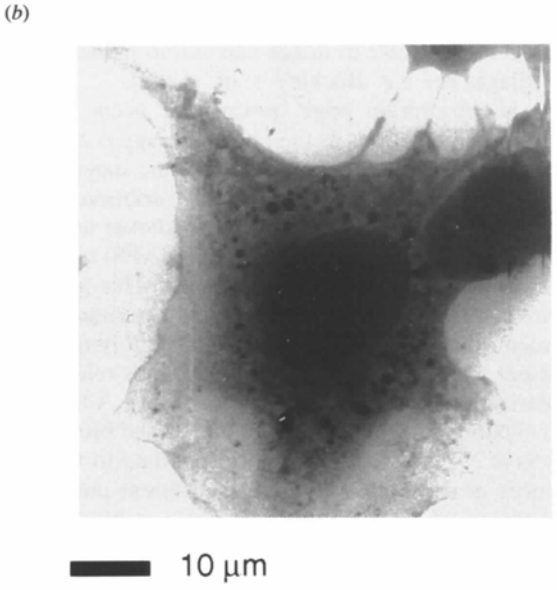
(b)
10 μm

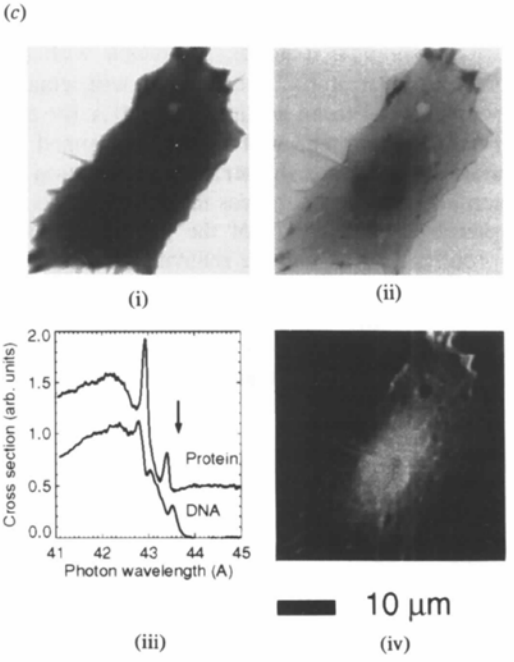
(c)
(i)
(ii)
Cross section (arb. units)
2.0
1.5
1.0
0.5
0.0
Protein
DNA
41
42
43
44
45
Photon wavelength (A)
(iii)
10 μm
(iv)

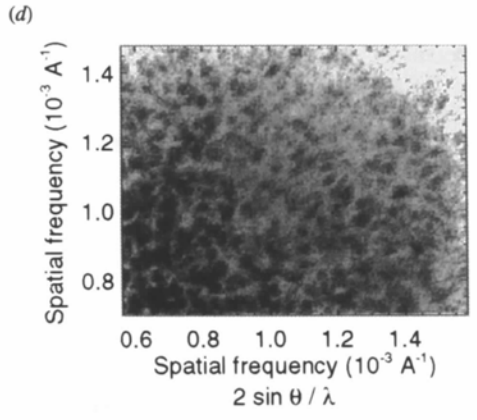
(d)
Spatial frequency (10-3 A-1)
1.4
1.2
1.0
0.8
0.6
0.8
1.0
1.2
1.4
Spatial frequency (10-3 A-1)
2 sin θ / λ

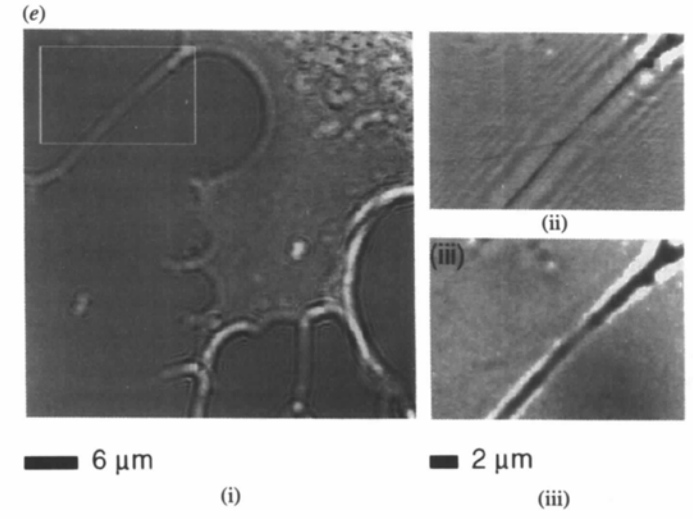
(e)
6 μm
(i)
(ii)
(iii)
2 μm
(iii)

radiation, whilst NEXAFS information can be extracted from the dependence of the spectrum on the incident X-ray energy. In the case of fluorescence, fluorescent yields are largest with higher-energy incident photons for which very high-resolution X-ray optics are not currently available; thus results, while analytically impressive (Bajt, Clark, Sutton, Rivers & Smith, 1993), are not currently able to exceed resolutions of about 2 μm (Yun, Viccaro, Chrzas & Lai, 1992). Recently, Kirz (1994) has initiated experiments to see whether lower-energy incident photons can be used, with lower yields but better resolution. In the case of electron emission (reviewed in Ade, 1992), scanning with zone-plate-focused soft X-rays in the Brookhaven SPEM has been used to obtain chemical and compositional information from the surfaces of aluminium and silicon at a resolution of 0.1–0.4 μm (Ade *et al.*, 1991). Other types of optics, including Schwarzschild mirror optics have also been used (Ng *et al.*, 1990).

V. Examples

This paper has dealt almost exclusively with the techniques, not the results, of X-ray microscopy. To conclude, in order to give some visual impression of the present capabilities of the field, Fig. 4 gives a very small sampling of examples of current work.

This paper owes a debt to many people, from the earlier workers in X-ray microscopy to our colleagues today in other centers world-wide. We wish to thank especially the members of our own group at Brookhaven and the State University of New York at Stony Brook; most particularly, Janos Kirz, Professor of Physics at Stony Brook, for many years of outstanding contributions to the field and for interest and encouragement in the preparation of this paper.

One of us (HC) acknowledges support by the US National Science Foundation (grant no. BIR-9316594). Our work on diffractive imaging is supported by grant no. DE-FG02-89ER60858 of the US Department of Energy.

Notes

1. *History of the subject, literature, research groups*

The history of X-ray microscopy goes back to 1896, the year following the discovery of X-rays by Röntgen. The method employed through the earlier years was microradiography, in which specimens were contact imaged at 1:1 on fine-grain film and the latter magnified in the optical microscope. The foundations of the modern work were laid following the Second World War (Kirkpatrick & Baez, 1948; Baez, 1952, 1961; Ladd, Hess & Ladd, 1956) when attention turned to methods that could exceed the optical microscope in resolution.

For a careful account of the earlier period and part of the later, see Cosslett & Nixon (1960). For a brief account that carries the history somewhat further into the present period, see Howells, Kirz, Sayre & Schmahl (1985). Several summary articles on X-ray microscopy have also appeared in recent years (Michette, 1988; Howells, Kirz & Sayre, 1991; Schmahl & Cheng, 1991; Kirz, Jacobsen & Howells, 1995). A useful entry into the recent research literature, and a guide to the groups (approximately 35 in 11 countries) working in the field, is provided through conference proceedings, including Schmahl & Rudolph (1984), Sayre, Howells, Kirz & Rarback (1988), Michette, Morrison & Buckley (1992), Jacobsen & Trebes (1992) and Erko & Aristov (1994).

2. *Choice of wavelengths; specimen size; potential of soft X-ray photons for low-intervention high-information-content imaging*

The question arises of where in the X-ray spectrum will be found the most suitable photons for microscopy? The text above has identified, but without giving reasons, the near soft X-ray region (wavelength roughly 10–50 Å) as the region of greatest interest. Fig. 5 shows perhaps the most basic reasons.

Fig. 4. A sampling of examples of X-ray microscopy. (*a*) Current optical performance, using high-resolution test objects. (i) A 128-period test object as imaged with STEM. (ii) As imaged with the STXM at Brookhaven, equipped with a 450 Å resolution zone plate. (iii) The image of (ii) after deconvolution based on the measured optical transfer function of the zone plate. (iv) A 100-period test object as imaged with the Göttingen transmission X-ray microscope equipped with a 300 Å zone plate fabricated at Göttingen. The XM images display resolutions in the range shown by the upper XM square in Fig. 1. (*b*) STXM image of a fixed wet JU56 (wallaby cell line) fibroblast. (*c*) STXM images of a critical-point-dried Chinese hamster ovary fibroblast. (i) Imaged at 42.94 Å. (ii) Imaged at 43.20 Å. (iii) Near-edge X-ray absorption fine structure (NEXAFS curves) of DNA and protein near the carbon absorption edge. The arrow shows the absorption edge of atomic carbon. (iv) Image derived from (*c*) (i)–(iii) (plus images at several further wavelengths) showing distribution of DNA in the cell. (*d*) and (*e*) Diffraction-based examples. (*d*) A small portion of the diffraction pattern observed at the NSLS X1A beamline from a single stationary *Minutocellus polymorphus* cell, using 18 Å X-rays and an apparatus similar to that of Fig. 2. The region of reciprocal space shown is indicated by the axes. The pattern was recorded on silver halide film; the film graininess can be seen but the fact that the pattern is continuous and contains a large amount of structural information can be seen. It may be noted that the information shows a correlation distance (the size-scale of the lumpiness or speckling of the pattern) of the order of several times 10^{-5}Å^{-1}, corresponding to the specimen size, which was approximately 3 μm. Overall, the pattern is recorded reasonably well to a distance from the origin of 3.3×10^{-3}Å^{-1} (resolution 300 Å); beyond this it begins to disappear in the rather high noise of the film used. Pattern has been observed to 140 Å resolution for single honeybee myofibrils (Fan, Yeh, Chapman & Sayre, 1994) and to 70 Å resolution for small diatoms. With a CCD detector, it is hoped that pattern will be visible to higher resolution. (*e*) (i) A Gabor hologram of part of a critical-point-dried Chinese hamster fibroblast cell, observed at 18.9 Å at the X1A beamline. The hologram was recorded on poly(methyl methacrylate) and read with an atomic force microscope. (ii) A numerical reconstruction, based on the above hologram. Only a region of the full reconstruction is shown, corresponding to the boxed region of the hologram. (iii) An optical micrograph ($100 \times \text{NA} = 0.90$) of the specimen in the same field as (ii). Note that features in the optical micrograph are also present in the reconstruction, such as the variation in intensity along the prominent fiber structure. Note also the improved resolution in the reconstruction as compared with the micrograph, as can be seen in the visibility of a finer fiber branching from the first. The twin image is seen in the reconstruction as a series of fringes; this could be removed by further processing. References: (*a*) Jacobsen *et al.* (1991), Zhang, Jacobsen & Williams (1992); (*c*) Kirz *et al.* (1994), Zhang *et al.* (1994); (*d*) Sayre (1991); (*e*) Lindaas (1994).

In addition, a number of other considerations also support the wavelength region indicated by Fig. 5.

(*a*) The wavelength region for which the properties of available materials are most favorable for making zone-plate focusing optics (these are important in several of the X-ray microscopies; see §II) is the same region as indicated in Fig. 5. Further, the use of a zone plate in scanning microscopes requires that the zone plate be coherently illuminated. This problem also is much simplified at the longer X-ray wavelengths.

(*b*) In microscopies relying on coherent scattering, it is important not to confuse Compton-scattered photons with the coherently scattered ones. This problem too is simplified at the longer wavelengths, where Compton scattering almost disappears. (See Fig. 6.)

(*c*) Damage minimization calls for choosing wavelengths at which the ratio of the number of occurrences of the imaging reaction to the energy deposited in the specimen is as large as possible. For imaging methods that are primarily photoabsorption based, this ratio improves with increasing wavelength (see Fig. 7). [However, for methods based on coherent scattering, the opposite is true; for these methods it would be desirable to use shorter wavelengths, at least to the extent that the other considerations (*a*, *b*, *d*) will allow. In the case of X-ray crystallography, those considerations for various reasons are not important, and there is no difficulty in moving to the least-damaging wavelengths at about 0.5 Å.]

(*d*) Last, and extremely important, is a detail which may be noted in Fig. 5: the non-smoothness of the penetration curve in the indicated wavelength region for X-ray microscopy. That region contains numerous important absorption edges, including the *K*-absorption edges (at 23, 31 and 44 Å) of the major biological constituents oxygen, nitrogen, and carbon; the feature appearing in the figure is the oxygen edge in the absorption spectrum of water. From 23 to 44 Å, water is thus abnormally transparent relative to the nitrogen- and carbon-containing constituents of biological materials, allowing such materials to retain imaging contrast even in their hydrated state. Thus, all versions of X-ray microscopy inherit the invaluable property of being compatible with the imaging of specimens in a fully hydrated state, a key factor in their status as low-intervention imaging methods. Other benefits of the complex behavior of reaction cross sections throughout the soft X-ray region, which allow X-ray microscopies to provide high-information-content imaging, are discussed in §IV.

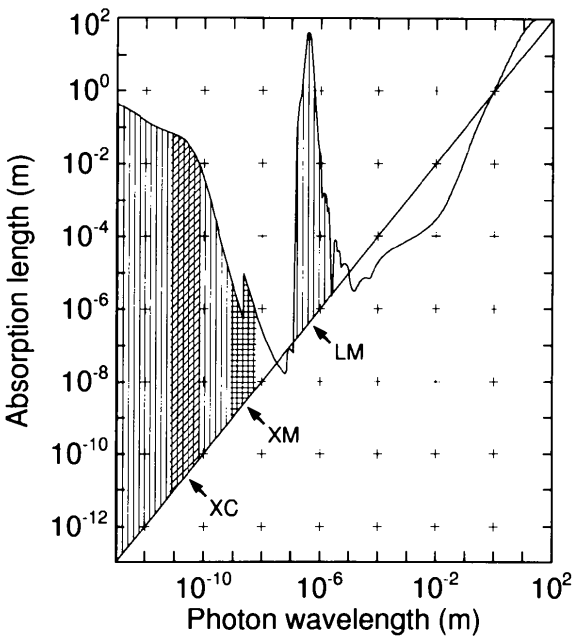

Fig. 5. Imaging regions for photons. The curved line plots the penetration depth of photons in water as a function of photon energy (Jackson, 1975; Henke, Gullikson & Davis 1993); water is chosen as a fairly typical biological dielectric (except for being unusually transparent in the visible). The straight line plots photon wavelength. The feasible regions for inducing and accurately locating internal photon reactions in a specimen are those in which the photon penetration depth is considerably in excess of the wavelength. Two such regions exist and are marked (vertical barring), and it is seen that visible or near-visible light and X-rays are the only candidates. (Thus, Fig. 1 does not omit any potential photon types that might be of use in imaging internal structure.) Since too much penetration can render specimens merely transparent, the optimal wavelength regions are those in which penetration depth is between 10^{2} and 10^{4} wavelengths, for example. (These factors are of course merely indicative.) This region is marked (horizontal barring) in the X-ray region and marks the roughly optimal area for X-ray microscopy. It turns out to lie between approximately 10 and 50 Å and to correspond to penetration depths or specimen thicknesses of the order of a few micrometers (compare with Fig. 1). For X-ray crystallography, where the specimen thickness must be increased relative to the imaging resolution to accommodate the periodicity of the specimen, it is reasonable to think in terms of penetration depths of 10^{8}–10^{10} wavelengths, and this region is also marked (slanted barring).

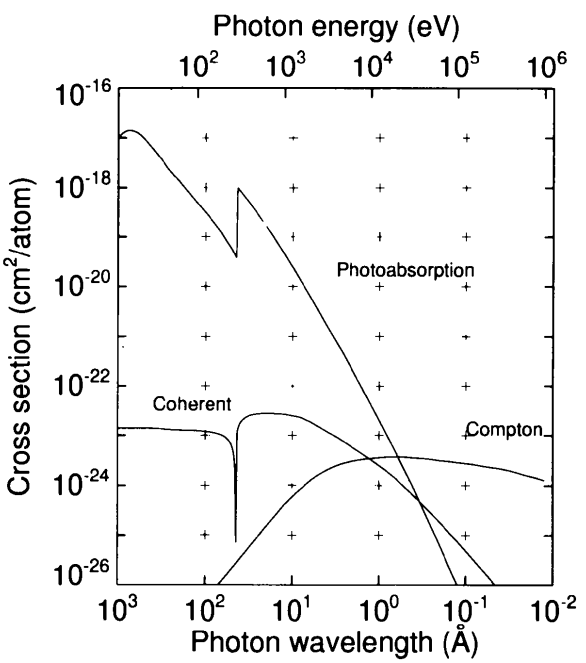

Fig. 6. The cross sections for the X-ray photon reactions with a carbon atom. The carbon absorption edge is visible in the photoabsorption and coherent scattering cross sections at 43.6 Å. [Additional near-edge fine structure occurs in bound carbon states but is not shown here; for this see §IV and Fig. 4(*c*) (iii).] The coherent scattering curve gives the squared magnitude of the complex coherent scattering factor (see text); no account is taken here of the possibility of coherency-based gain, which can occur in multi-atom structures (see *Note* 3). The data are from Henke, Gullikson & Davis (1993) and Hubbell *et al.* (1975).

3. *Addition rules for the photon reactions in multi-atom structures; coherency gain; reaction location from coherently scattered particles*

The reaction cross sections of Fig. 6 are for single carbon atoms. Real specimens, however, are N-atom structures.

In an N-atom structure, atomic cross sections (reaction areas) add algebraically in the case of photoabsorption and Compton scattering:

$$\Omega = \sum_{j=1}^{N} \sigma_j ;$$

while, in the case of coherent scattering, atomic scattering factors (reaction lengths) add vectorially with path lengths taken into account, giving

$$F(\mathbf{u}, \mathbf{u}_0) = \sum_{j=1}^{N} f_j \exp[i2\pi \mathbf{r}_j \cdot (\mathbf{u} - \mathbf{u}_0)/\lambda]$$

(where $\mathbf{u}_0$ and $\mathbf{u}$ are unit vectors giving the directions of incident and scattered photons and f_j and $\mathbf{r}_j$ are the scattering factor and location of the jth atom), followed by squaring to obtain the N-atom scattering cross section

$$\Omega(\mathbf{u}, \mathbf{u}_0) = |F(\mathbf{u}, \mathbf{u}_0)|^2.$$

Thus, for coherent scattering, Ω shows interference effects that depend upon $\mathbf{r}_j$.

This difference leads to important differences in terms of imaging. One concerns reaction counts and arises from the fact that the cross sections for coherent scattering at the atomic level, $|f_j|^2$, are troublesomely small from the point of view of observing the scattering experimentally and would remain so at the N-atom level as well were it not for the addition rule, which allows Ω to grow approximately as N^2 in directions $\mathbf{u}$ where path-length considerations allow the photons from N scatterers to interfere constructively, rather than simply as N. In cases where N is large, therefore, there can be a large amplification of signal strength (*i.e.* a coherency-based gain $C \simeq N$), which is available when the coherently scattered photons are being used for imaging, and which is not available to the other reaction effects. This point, fortunate for coherent scattering as a basis for imaging, will be returned to in §III in connection with the question of imaging dosage.

The other point that flows from the addition rules is that in the scattering of coherent photons there is an almost immediate method for finding the reaction locations $\mathbf{r}_j$, namely measurement of $\Omega(\mathbf{u}, \mathbf{u}_0)$, followed by phasing of $F = \Omega^{1/2}$ and Fourier inversion. This is of course the method first developed in X-ray crystallography. (However, it is not limited to the case of crystallographic specimens; in an important respect, namely the problem of phasing, it is actually stronger in the non-crystallographic situation, as will be seen in §II.4.) In this method, it is the photons and the structure itself that 'sense' the scattering positions, and do so with very high $(\lambda/2)$ accuracy, without major assistance from the instrumentation. In contradistinction, the other reaction effects get no such help from their addition rule and the instrumentation itself must supply the necessary highly accurate sense of position.

4. *Contrast in biological specimens*

The choice of $R = 10^4$ (1% noise level) may be insufficient for good imaging if the specimen shows poor contrast for the imaging reaction chosen. [Letting contrast $= \langle \Delta p \rangle / \langle p \rangle$, where $\langle \Delta p \rangle$ and $\langle p \rangle$ are the spread and mean of the probabilities of the occurrence of the reaction in the resolution elements of the specimen, R should include a factor of 1/contrast^2 to keep imaging quality constant with varying contrast.] However, in the calculations that follow, it is assumed that a constant value of $R = 10^4$ will suffice. To make this assumption justified, X-ray wavelengths of 30 and 23 Å have been chosen for the calculations on photoabsorption imaging and coherent scattering imaging, respectively, those being wavelengths at which contrast is high for these reactions even in hydrated biological specimens.

In the later calculation on X-ray crystallography, there is no problem in assuming contrast to be high, as contrast is assured at atomic or near-atomic resolution.

5. *Number of reactions per deposited* eV

Fig. 7 gives useful data on reactions and energy cost.

6. *Volume of the resolution element*

We find that even though the illumination of a sample and photon paths within a sample are different for various X-ray microscopy techniques, the volume, V, of the resolution element is approximately the same for a given imaging resolution, in the case where the specimen is viewed in a single orientation (*i.e.* no attempt is made to image the specimen at a number of rotated or longitudinally translated positions).

In contact microscopy, the resolution depends on the thickness of the sample, and the resolution due to blurring by diffraction from a layer at height h from the recording medium is approximately $(h\lambda)^{1/2}$. Thus, if the height is optimized to the resolution so that $d = (h\lambda)^{1/2}$, then $V = hd^2 = d^4/\lambda$. In

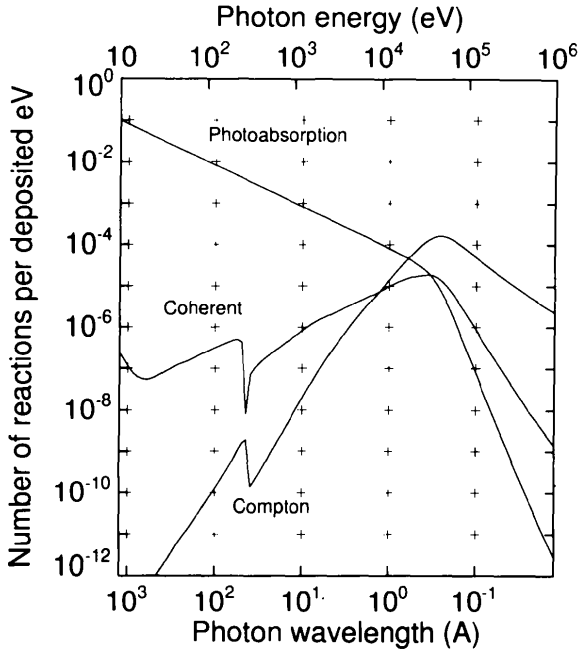

Fig. 7. Number of reactions occurring in carbon per deposited eV. The quantity E in the text is the reciprocal of this quantity. In the curve for coherent scattering, it is assumed that no coherency gain is present ($C = 1$). Data are based on the cross sections of Fig. 6 and on Evans (1958).

scanning and transmission microscopy, the transverse resolution is given by $d = \lambda/\mathrm{NA}$, where NA is the numerical aperture of the zone plate, and the longitudinal resolution is $\lambda/(\mathrm{NA})^2 = d^2/\lambda$. Combining these, we obtain the same volume of the resolution element. In diffraction or holography, the imaging is never purely projective (the data lie on the reflecting sphere). As the transverse resolution d decreases, the resolution element changes shape, from prolate (transverse resolution better than longitudinal) to oblate, with the transition occurring at $d \simeq \lambda$. The expression $V = d^2[d(d/\lambda)] = d^4/\lambda$ roughly expresses this. Note that, in all these cases, for practical values of specimen thickness, d, and λ, the specimen thickness is normally larger than (*i.e.* drops out in comparison with) the resolution-element thickness d^2/λ. Therefore, for specimens thinner than about 3 μm, the curves in Fig. 3 cannot be extrapolated to resolutions d larger than shown.

As noted above, single-orientation imaging is assumed, and the images produced are two-dimensional (except in holography and diffraction where some three-dimensionality of the image occurs). For three-dimensional imaging, some form of multiple-exposure imaging (imaging in multiple orientations or serial focusing) is employed. This is reflected a little later in the text with the introduction of an additional factor M.

7. *Coherency gain in the crystal case*

If a structure is periodic, with U copies of an n-atom unit cell, then for the Bragg directions the coherent scattering addition rule (*Note* 3) becomes

$$F(\mathbf{u}, \mathbf{u}_0) = U \sum_{j=1}^{n} f_j \exp[i2\pi r_j \cdot (\mathbf{u} - \mathbf{u}_0)/\lambda];$$

i.e., for a crystal, $\Omega(\mathbf{u}, \mathbf{u}_0)$ in all Bragg directions grows as U^{2n} and not merely as N $(= Un)$. Thus, periodicity produces an additional very large coherency gain $C = U$ for coherent scattering in the Bragg directions. This gain is constant and does not decrease with increasing resolution, thus allowing X-ray crystallography to image to high resolutions.

8. *Additional comments on diffractive methods*

There are two main problems faced by methods that image on the basis of diffraction effects. First, there is a need to secure as much coherent gain as possible because in its absence the effects are sufficiently weak and have a high enough energy cost per reaction to produce an unfavorable damage limitation on resolution. Second, there is a need to avoid specimens that contain copies of the structure of interest in too many different orientations; although the copies are separated in direct space, in Fourier space their transforms are translated to the origin, where they can overlap so confusingly that true imaging of the structure (which is equivalent to disentangling of the transforms) is prevented.

The solution to these needs provided by X-ray crystallography is extremely effective. A huge coherency gain is secured (see *Note* 7), giving the technique its pre-eminent position in terms of resolution; and the structure to be imaged is present in only a few orientations, so that the orientational problem can usually be dealt with and the structure solved. It should be noted, however, that the use of a crystalline specimen entails a non-negligible price. One price is that the Bragg sampling density is just sufficient for imaging when phases are present but produces a major informational deficit in terms of imaging when they are not. It is fortunate that crystallographers have been highly successful in finding ways to incorporate enough supplementary information to make good the deficit (*i.e.* 'solve the phase problem'); the continuing cost of these additional required procedures in crystallography is, however, far from negligible. The other price is the required crystallizability of the structure that it is desired to image. Today, this may be the more serious limitation on the long-term future of X-ray crystallography.

What is novel in the diffractive methods being developed in X-ray microscopy is the idea that one further type of specimen – the single-copy specimen such as a single biological cell – can also be fully imaged by diffractive methods. Its great advantage is its ready availability even for structures of very large size, and its secondary advantage is the immediate entry into phasing and imaging that its continuous unsampled Fourier transform gives. Its disadvantage is that it deals only partially with the reaction-weakness problem; the coherency gain is only of the order of the number of atoms in the resolution element, which decreases with increasing resolution, and results in the moderate resolutions estimated in Fig. 3.

9. *Specimen periodicity and imaging*

As stated in the *Introduction*, one of the objectives of this paper has been to study how the presence or absence of specimen periodicity affects specimen imaging and to do so using a common vocabulary and viewpoint; *i.e.* to be in a position to state some of the relationships between X-ray crystallography and microscopy from a unified point of view. It is our hope that such a contribution will prove helpful to communicate between the two imaging communities.

With this in mind, let us briefly summarize the situation as we see it. Given the basic starting point that imaging involves the production of reactions in a specimen, photon-penetration considerations favor soft X-rays and μm-range specimens for nonperiodic specimens, with harder X-rays being preferred for periodic specimens (Fig. 5). From this point on, the principles of the two cases remain the same but the practice separates. In the periodic case, the periodicity provides one reaction (coherent scattering) with very high signal-strength gain; this basically determines X-ray crystallography as a diffraction-based comparatively low dosage method, able for these reasons to operate at high resolution (Fig. 3) but limited to structure sizes small enough to allow crystallization. In the nonperiodic case, very high gain mechanisms are absent, dosages are higher and this plus the longer wavelengths produces lower resolutions. At the same time, structures can be very large and the longer wavelengths permit the alternative of focusing-based imaging and provide a richness of reaction types, which allows the imaging of specimens in their natural state as well as the mapping of the chemical state in such specimens. X-ray crystallography has long since proved its value to science and continues to do so today; X-ray microscopy is now nearing the point where its value can begin to be determined.

References

ADE, H. (1992). *Nucl. Instrum. Methods*, A**319**, 311–319.

ADE, H. & HSIAO, B. (1993). *Science*, **262**, 1427–1429.

ADE, H., KIRZ, J., HULBERT, S., JOHNSON, E., ANDERSON, E. & KERN, D. (1991). *J. Vac. Sci. Technol.* A**9**, 1902–1906.

ADE, H., ZHANG, X., CAMERON, S., COSTELLO, C., KIRZ, J. & WILLIAMS, S. (1992). *Science*, **258**, 972–975.

ARISTOV, V. V. (1994). In *X-ray Microscopy*. IV, edited by A. I. ERKO & V. V. ARISTOV. Chernogolovka, Russia: Bogorodski Pechatnik Publishing Co. To be published.

ATTWOOD, D. (1994). In *X-ray Microscopy*. IV, edited by A. I. ERKO & V. V. ARISTOV. Chernogolovka, Russia: Bogorodski Pechatnik Publishing Co. To be published.

BAEZ, A. V. (1952). *J. Opt. Sci. Am.* **42**, 756–762.

BAEZ, A. V. (1961). *J. Opt. Sci. Am.* **51**, 405–412.

BAJT, S., CLARK, S. B., SUTTON, S. R., RIVERS, M. L. & SMITH, J. V. (1993). *Anal. Chem.* **65**, 1800–1804.

BATES, R. H. T. (1982). *Optik (Stuttgart)*, **61**, 247–262.

BENNETT, P. M., FOSTER, G. F., BUCKLEY, C. J. & BURGE, R. E. (1993). *J. Microsc.* **172**, 109–119.

BUCKLEY, C. J., BELLAMY, S. J., KHALEQUE, N., DOWNES, S. & ZHANG, X. (1994). In *X-ray Microscopy*. IV, edited by A. I. ERKO & V. V. ARISTOV. Chernogolovka, Russia: Bogorodski Pechatnik Publishing Co. To be published.

BUCKLEY, C. J., FOSTER, G. F., BURGE, R. E., ALI, S. Y., SCOTCHFORD, C. A., KIRZ, J. & RIVERS, M. L. (1992). *Rev. Sci. Instrum.* **63**, 588–590.

CHAPMAN, H. N. (1995). In preparation.

CHAPMAN, H. N., BALHORN, R., HUD, N., FAN, S. F., SAYRE, D. & YEH, Y. (1993). Unpublished.

COSSLETT, V. E. & NIXON, W. C. (1960). *X-ray Microscopy*. Cambridge Univ. Press.

COTTON, R. A., DOOLEY, M. D., FLETCHER, J. H., STEAD, A. D. & FORD, T. W. (1992). In *Soft X-ray Microscopy. Proc. SPIE* No. 1741, pp. 204–212.

DAVID, C., FAY, N., MEDENWALDT, R. & THIEME, J. (1994). In *X-ray Microscopy*. IV, edited by A. I. ERKO & V. V. ARISTOV. Chernogolovka, Russia: Bogorodski Pechatnik Publishing Co. To be published.

DAVID, C., MEDENWALDT, R., THIEME, J., GUTTMANN, P., RUDOLPH, D. & SCHMAHL, G. J. (1992). *Optics (Paris)*, **23**, 255–258.

ECHLIN, P. (1992). *Low-Temperature Microscopy and Analysis*. New York: Plenum Press.

ERKO, A. I. & ARISTOV, V. V. (1994). Editors. *X-ray Microscopy*. IV. Chernogolovka, Russia: Bogorodski Pechatnik Publishing Co. To be published.

EVANS, R. D. (1958). In *Handbuch der Physik*, Vol. 34, edited by S. FLUGGE. Berlin: Springer.

FAN, S. F., YEH, Y., CHAPMAN, H. N. & SAYRE, D. (1994). Work in progress.

FENIMORE, E. E. & CANNON, T. M. (1978). *Appl. Opt.* **178**, 337–347.

FLETCHER, J., COTTON, R. & WEBB, C. (1992). In *Soft X-ray Microscopy. Proc. SPIE* No. 1741, pp. 142–153.

GOODMAN, J. W. (1968). *Introduction to Fourier Optics*. New York: McGraw-Hill.

HARDING, G., STRECKER, H. & TISCHLER, R. (1983/84). *Phillips Tech. Rev.* **41**, 46–59.

HAYES, M. H. (1982). *IEEE Trans. Acoust. Speech Signal Process.* ASSP-**30**, 140–154.

HEGERL, R. & HOPPE, W. (1976). *Z. Naturforsch.* **31**, 1717–1721.

HENKE, B. L., GULLIKSON, E. M. & DAVIS, J. C. (1993). *At. Data Nucl. Data Tables*, **54**, 181–342.

HOPE, H. (1990). *Ann. Rev. Biophys. Biophys. Chem.* **19**, 107–126.

HOWELLS, M. R., KIRZ, J. & SAYRE, D. (1991). *Sci. Am.* **264**(2), 88–94.

HOWELLS, M. R., KIRZ, J., SAYRE, D. & SCHMAHL, G. (1985). *Phys. Today*, **38**(8), 22–32.

HUBBELL, J. H., VIEGELE, W. J., BRIGGS, E. A., BROWN, R. T., CROMER, D. T. & HOWERTON, R. J. (1975). *J. Phys. Chem. Ref. Data*, **4**, 471–538.

IDELL, P. J. (1994). Editor. *Digital Image Recovery and Synthesis*. II. *Proc. SPIE* No. 2029.

JACKSON, J. D. (1975). *Classical Electrodynamics*, p. 291. New York: John Wiley.

JACOBSEN, C. (1992). *X-ray Microscopy*. III. *Springer Series in Optical Sciences*, Vol. 67, pp. 274–277. Berlin: Springer

JACOBSEN, C., ANDERSON, E., CHAPMAN, H., KIRZ, J., LINDAAS, S., RIVERS, M., WANG, S., WILLIAMS, S., WIRICK, S. & ZHANG, X. (1994). In *X-ray Microscopy*. IV, edited by A. I. ERKO & V. V. ARISTOV. Chernogolovka, Russia: Bogorodski Pechatnik Publishing Co. To be published.

JACOBSEN, C., HOWELLS, M., KIRZ, J. & ROTHMAN, S. (1990). *J. Opt. Soc. Am.* A7, 1847–1861.

JACOBSEN, C. & TREBES, J. (1992). Editors. *Soft X-ray Microscopy. Proc. SPIE* No. 1741.

JACOBSEN, C., WILLIAMS, S., ANDERSON, E., BROWNE, M. T., BUCKLEY, C. J., KERN, D., KIRZ, J., RIVERS, M. & ZHANG, X. (1991). *Opt. Commun.* **86**, 351.

KIRKPATRICK, P. & BAEZ, A. V. (1948). *J. Opt. Sci. Am.* **38**, 766–774.

KIRZ, J. (1974). *J. Opt. Sci. Am.* **64**, 301–309.

KIRZ, J. (1994). Private communication.

KIRZ, J., ADE, H., BOTTO, R. E., CODY, G. D., FU, J., JACOBSEN, C., LINDAAS, S., MANGEL, W. F., MCGRATH, W. J., OEHLER, V., VAN'T HOF, J., WILLIAMS, S., WIRICK, S. & ZHANG, X. (1994). In *X-ray Microscopy*. IV, edited by A. I. ERKO & V. V. ARISTOV. Chernogolovka, Russia: Bogorodski Pechatnik Publishing Co. To be published.

KIRZ, J., JACOBSEN, C. & HOWELLS, M. (1995). *Q. Rev. Biophys.* Submitted.

LADD, W. A., HESS, W. M. & LADD, M. W. (1956). *Science*, **123**, 370–371.

LINDAAS, S. (1994). PhD thesis, State Univ. of New York at Stony Brook, New York, USA.

MCNULTY, I. (1994). *Proceedings of Conference on Synchrotron Radiation Instrumentation* 8, edited by G. G. LONG, D. R. MUELLER & S. H. SOUTHWORTH. *Nucl. Instrum. Methods*, A**347**, 170–176.

MCNULTY, I., KIRZ, J., JACOBSEN, C., ANDERSON, E. H., HOWELLS, M. R. & KERN, D. P. (1992). *Science*, **256**, 1009–1012.

MASER, J. (1994). In *X-ray Microscopy*. IV, edited by A. I. ERKO & V. V. ARISTOV. Chernogolovka, Russia: Bogorodski Pechatnik Publishing Co. To be published.

MASER, J. & SCHMAHL, G. (1992). *Opt. Commun.* **89**, 355–362.

MICHETTE, A. G. (1986). *Optical Systems for Soft X-rays*. New York: Plenum Press.

MICHETTE, A. G. (1988). *Rep. Prog. Phys.* **51**, 1525–1606.

MICHETTE, A. G., MORRISON, G. R. & BUCKLEY, C. J. (1992). Editors. *X-ray Microscopy*. III. *Springer Series in Optical Sciences*, Vol. 67. Berlin: Springer.

NG, W., RAY-CHAUDHURI, A. K., CROSSLEY, S., CROSSLEY, D., GONG, C., GUO, J., HANSEN, R. W. C., MARGARITONDO, G., CERRINA, F., UNDERWOOD, J. H., PERERA, R. C. C. & KORTWRIGHT, J. (1990). *J. Vac. Sci. Technol.* A**8**, 2563–2565.

NUGENT, K. A. (1992). *Phys. Rev. Lett.* **68**, 2261–2264.

NUGENT, K. A., CHAPMAN, H. N. & KATO, Y. (1991). *J. Mod. Opt.* **38**, 1957–1971.

PALMER, J. R. & MORRISON, G. R. (1992). In *X-ray Microscopy*. III. *Springer Series in Optical Sciences*, Vol. 67, pp. 278–280. Berlin: Springer.

RAY, J. H. (1954). MSc thesis, Univ. Pennsylvania, Pittsburgh, USA.

RODENBURG, J. M. & BATES, R. H. T. (1992). *Philos. Trans. R. Soc. London Ser. A*, **339**, 521–553.

RUDOLPH, D., SCHMAHL, G. & NIEMANN, B. (1990). In *Modern Microscopies*, edited by P. J. DUKE. & A. G. MICHETTE. New York: Plenum Press.

SAYRE, D. (1980). In *Imaging Processes and Coherence in Physics. Springer Lecture Notes in Physics*, Vol. 112, edited by M. SCHLENKER, M. FINK, J. P. GOEDGEBUER, C. MALGRANGE, J. C. VIÉNOT & R. H. WADE, pp. 229–235. Berlin: Springer.

SAYRE, D. (1986). Proc. Am. Crystallogr. Assoc. Meet. Abstr., p. 42.

SAYRE, D. (1988). In *X-ray Microscopy*. II. *Springer Series in Optical Sciences*, Vol. 56, pp. 173–177. Berlin: Springer.

SAYRE, D. (1991). *Direct Methods of Solving Crystal Structures*, edited by H. SCHENK, pp. 353–356. New York: Plenum Press.

SAYRE, D., HOWELLS, M., KIRZ, J. & RARBACK, H. (1988). Editors. *X-ray Microscopy*. II. *Springer Series in Optical Sciences*, Vol. 56. Berlin: Springer.

SAYRE, D., YUN, W. B. & KIRZ, J. (1988). *X-ray Microscopy*. II. *Springer Series in Optical Sciences*, Vol. 56, pp. 272–275. Berlin: Springer.

SCHMAHL, G. & CHENG, P. C. (1991). In *Handbook of Synchrotron Radiation*, Vol. 4, edited by S. EBASHI, M. KOCH & E. RUBENSTEIN. Amsterdam: Elsevier.

SCHMAHL, G., GUTTMANN, P., SCHNEIDER, G., NIEMANN, B., DAVID, C., WILHEIN, T., THIEME, J. & RUDOLPH, D. (1994). In *X-ray Microscopy*. IV, edited by A. I. ERKO & V. V. ARISTOV. Chernogolovka, Russia: Bogorodski Pechatnik Publishing Co. To be published.

SCHMAHL, G., NIEMANN, B., RUDOLPH, D., DIEHL, M., THIEME, J., NEFF, W., HOLZ, R., LEBERT, R., RICHTER, F. & HERZIGER, G. (1992). *X-ray Microscopy*. III. *Springer Series in Optical Sciences*, Vol. 67, edited by A. G. MICHETTE, G. R. MORRISON & C. J. BUCKLEY, pp. 66–69. Berlin: Springer.

SCHMAHL, G. & RUDOLPH, D. (1984). *X-ray Microscopy*. *Springer Series in Optical Sciences*, Vol. 43. Berlin: Springer.

SCHMAHL, G. & RUDOLPH, D. (1987). *X-ray Microscopy*, edited by P. C. CHENG & G. JAN, pp. 231–238. Berlin: Springer.

SCHMAHL, G., RUDOLPH, D. & GUTTMANN, P. (1988). In *X-ray Microscopy*. II. *Springer Series in Optical Sciences*, Vol. 56, edited by D. SAYRE, M. HOWELLS, J. KIRZ & H. RARBACK, pp. 228–232. Berlin: Springer.

SCHMAHL, G., RUDOLPH, D., NIEMANN, B., GUTTMANN, P., THIEME, J., SCHNEIDER, G., DAVID, C., DIEHL, M. & WILHEIN, T. (1993). *Optik (Stuttgart)*, **93**, 95–102.

SCHNEIDER, G. (1994). In *X-ray Microscopy*. IV, edited by A. I. ERKO & V. V. ARISTOV. Chernogolovka, Russia: Bogorodski Pechatnik Publishing Co. To be published.

SHEALY, D. L., WANG, C., JIANG, W., JIN, L. & HOOVER, R. B. (1992). *Soft X-ray Microscopy*. *Proc. SPIE* No. 1741, edited by C. JACOBSEN & J. TREBES, pp. 20–31.

SHINOZAKI, D. M., CHENG, P. C. & LIN, T. H. (1992). *X-ray Microscopy*. III. *Springer Series in Optical Sciences*, Vol. 67, edited by A. G. MICHETTE, G. R. MORRISON & C. J. BUCKLEY, pp. 329–334. Berlin: Springer.

SKINNER, C. H., DICICCO, D. S., KIM, D., ROSSER, R. J., SUCKEWER, S., GUPTA, A. P. & HIRSCHBERG, J. G. (1990). *J. Microsc.* **159**, pp. 51–60.

SKINNER, G. K. (1988). *Sci. Am.* **259**(2), 66–71.

SOLEM, J. C. & BALDWIN, G. C. (1982). *Science*, **218**, 229–235.

SPILLER, E. & FEDER, R. (1977). *X-ray Optics*. *Springer Topics in Applied Physics*, Vol. 22, edited by H.-J. QUEISSER, pp. 35–92. Berlin: Springer.

TOMIE, T., SHIMIZU, H., MAJIMA, T., YAMADA, M., KANAYAMA, T., KONDO, H., YANO, M. & ONO, M. (1991). *Science*, **252**, 691–693.

WILLIAMS, S., ZHANG, X., JACOBSEN, C., KIRZ, J., LINDAAS, S., VAN'T HOF, J. & LAMM, S. S. (1993). *J. Microsc.* **170**, 155–165.

YUN, W. B., KIRZ, J. & SAYRE, D. (1987). *Acta Cryst.* A**43**, 131–133.

YUN, W. B., VICCARO, P. J., CHRZAS, J. & LAI, B. (1992). *Rev. Sci. Instrum.* **63**, 582–585.

ZHANG, X., JACOBSEN, C. & WILLIAMS, S. (1992). *Soft X-ray Microscopy*. *Proc. SPIE* No. 1741, pp. 251–259.

ZHANG, X., WILLIAMS, S., JACOBSEN, C., KIRZ, J., FU, J. & WIRICK, S. (1994). In preparation.